Published in final edited form as:
Science. 2013 June 14; 340(6138): 1330–1333. doi:10.1126/science.1238880.

Targeting Isoprenylcysteine Methylation Ameliorates Disease in a Mouse Model of Progeria

Mohamed X. Ibrahim[1], **Volkan I. Sayin**[1], **Murali K. Akula**[1], **Meng Liu**[1,2], **Loren G. Fong**[3], **Stephen G. Young**[3], and **Martin O. Bergo**[1,*]

[1]Sahlgrenska Cancer Center, Department of Molecular and Clinical Medicine, Institute of Medicine, Sahlgrenska Academy, University of Gothenburg, S-41390 Gothenburg, Sweden.

[2]Department of Clinical Chemistry and Transfusion Medicine, Institute of Biomedicine, Sahlgrenska Academy, University of Gothenburg, S-41345 Gothenburg, Sweden.

[3]Departments of Medicine and Human Genetics, David Geffen School of Medicine, University of California, Los Angeles, CA 90095, USA.

Abstract

Several progeroid disorders, including Hutchinson-Gilford progeria syndrome (HGPS) and restrictive dermopathy (*ZMPSTE24* deficiency), arise when a farnesylated and methylated form of prelamin A accumulates at the nuclear envelope. Here, we found that a hypomorphic allele of isoprenylcysteine carboxyl methyltransferase (ICMT) increased body weight, normalized grip strength, and prevented bone fractures and death in *Zmpste24*-deficient mice. The reduced ICMT activity caused prelamin A mislocalization within the nucleus and triggered prelamin A–dependent activation of AKT-mammalian target of rapamycin (mTOR) signaling, which abolished the premature senescence of *Zmpste24*-deficient fibroblasts. ICMT inhibition increased AKT-mTOR signaling and proliferation and delayed senescence in human HGPS fibroblasts but did not reduce the levels of misshapen nuclei in mouse and human cells. Thus, targeting ICMT might be useful for treating prelamin A–associated progeroid disorders.

Children with Hutchinson-Gilford progeria syndrome (HGPS) exhibit premature aging phenotypes and often die during their teenage years. HGPS is caused by mutations in the gene encoding prelamin A and lamin C (*LMNA*) that result in an internally truncated form of prelamin A (called progerin) that accumulates at the nu clear rim and induces nuclear shape abnormalities (1–4). Progerin retains its carboxyl-terminal *CAAX* motif, which triggers farnesylation of the cysteine (i.e., the "*C*" in the *CAAX* motif) by protein farnesyltransferase (FTase) (fig. S1). Interfering with farnesylation with an FTase inhibitor (FTI) reduces the frequency of misshapen nuclei in *Zmpste24*-deficient fibroblasts and HGPS fibroblasts and ameliorates disease phenotypes in *Zmpste24*-deficient mice and other models of HGPS, although the benefits are modest (2, 5–10). A recent clinical trial of an FTI in children with HGPS showed a modest beneficial effect on disease phenotypes (11, 12).

*Corresponding author. martin.bergo@gu.se.

After farnesylation, the last three amino acids (the "*AAX*" of the *CAAX* motif) of prelamin A and progerin are clipped off, and the farnesylcysteine is methylated by isoprenylcysteine carboxyl methyltransferase (ICMT) (fig. S1). Methylation of some *CAAX* proteins, including the RAS oncoprotein, is important for proper targeting to membranes within cells (13, 14), but the relevance of methylation to prelamin A–associated progeroid disorders is unknown. To address this issue, we took advantage of a hypomorphic *Icmt* allele ($Icmt^{hm}$), fortuitously created by the insertion of *loxP* sites flanking exon 1 of *Icmt* (14, 15). $Icmt^{hm/hm}$ mice were leaner than $Icmt^{hm/+}$ littermates (fig. S2, A to D) but were healthy and lived for >2 years. The reduced ICMT expression in $Icmt^{hm/hm}$ cells inhibited prelamin A processing to lamin A (fig. S2E).

We bred $Zmpste24^{-/-}$ mice harboring the $Icmt^{hm}$ allele. ICMT expression and activity levels were 70 to 90% lower in $Zmpste24^{-/-}Icmt^{hm/hm}$ mice than in $Zmpste24^{-/-}Icmt^{+/+}$ littermates (fig. S3, A to D). Incubating $Zmpste24^{-/-}Icmt^{hm/hm}$ fibro-blasts with a Cre-adenovirus (adCre) eliminated ICMT expression (fig. S3, B and D). The reduced ICMT activity in $Zmpste24^{-/-}Icmt^{hm/hm}$ livers resulted in a moderate accumulation of ICMT substrates (fig. S3E). To determine whether prelamin A existed in unmethylated form in $Zmpste24^{-/-}Icmt^{hm/hm}$ cells, we performed mass spectrometry of prelamin A in isolated fibro-blast nuclei (fig. S3F). The relative levels of unmethylated prelamin A were higher in nuclei of $Zmpste24^{-/-}Icmt^{hm/hm}$ and $Zmpste24^{-/-}Icmt^{\Delta/\Delta}$ cells than in $Zmpste24^{-/-}Icmt^{+/+}$ cells (fig. S3G).

As expected, $Zmpste24^{-/-}Icmt^{+/+}$ mice developed alopecia, a hobbling gait, growth retardation, and reduced grip strength; they began to die at ~10 weeks of age (16–18) (Fig. 1, A to D, and fig. S4). By 30 weeks, all had died or been euthanized (Fig. 1D). At that time, $Zmpste24^{-/-}Icmt^{+/+}$ mice had multiple rib fractures adjacent to the costovertebral joints (Fig. 1, E and F). L2 ver tebrae from $Zmpste24^{-/-}Icmt^{+/+}$ mice exhibited osteopenia and reduced osteoid, suggesting little or no ongoing bone formation (fig. S5A). In contrast, all $Zmpste24^{-/-}Icmt^{hm/hm}$ mice were alive at 30 weeks, and their gait, grip strength, fur, and body-weight curves were much better than in $Zmpste24^{-/-}Icmt^{+/+}$ mice (Fig. 1, A to D, and fig. S4).

All $Zmpste24^{-/-}Icmt^{hm/hm}$ mice were sacrificed at 30 weeks of age, and none had rib fractures (Fig. 1, E and F). Osteoblasts in L2 vertebrae of $Zmpste24^{-/-}Icmt^{hm/hm}$ mice were six times as abundant as in $Zmpste24^{-/-}Icmt^{+/+}$ mice; osteoclast numbers were unchanged (Fig. 1, G and H, and fig. S5B). The numbers, thickness, and bone volume of trabeculae were higher in $Zmpste24^{-/-}Icmt^{hm/hm}$ mice than in $Zmpste24^{-/-}Icmt^{+/+}$ mice (fig. S5B). Moreover, at 13 to 15 weeks of age, $Zmpste24^{-/-}Icmt^{hm/hm}$ mice had increased mineral density and bone content (fig. S6A), as judged by dual x-ray absorptiometry (DXA). The DXA scans also revealed increased adipose tissue in $Zmpste24^{-/-}Icmt^{hm/hm}$ mice; however, total body weight at that time point did not differ (fig. S6B), consistent with the body-weight curves (Fig. 1B and fig. S4).

Misshapen nuclei are a hallmark of progeria cells. We initially suspected that the improved disease phenotypes of $Zmpste24^{-/-}Icmt^{hm/hm}$ mice would be accompanied by a lower frequency of misshapen nuclei in cultured fibroblasts, but this was not the case (Fig. 2, A

and B). In control experiments, knockout of Fntb (encoding the FTase β-subunit) in *Zmpste24*$^{-/-}$ fibroblasts reduced the frequency of misshapen nuclei to wild-type levels (fig. S7A).

We next determined whether reduced *Icmt* expression affects localization of prelamin A in *Zmpste24*$^{-/-}$ cells. Consistent with earlier studies (17, 18), prelamin A was mainly found at the nuclear rim in *Zmpste24*$^{-/-}$*Icmt*$^{+/+}$ hepatocytes, colocalizing with LAP2b (Fig. 2C). In contrast, prelamin A in *Zmpste24*$^{-/-}$*Icmt*$^{hm/hm}$ hepatocytes was abundant in the nucleoplasm (Fig. 2C and fig. S7B). Similar results were observed in skeletal muscle (fig. S7C). Prelamin A, which accumulated at moderate levels in *Zmpste24*$^{+/+}$*Icmt*$^{hm/hm}$ fibroblasts (fig. S2E), was entirely nucleoplasmic in liver sections (fig. S7D). The ratio of prelamin A and β-tubulin was similar in lysates of *Zmpste24*$^{-/-}$*Icmt*$^{hm/hm}$ and *Zmpste24*$^{-/-}$*Icmt*$^{+/+}$ tissues (fig. S7E). Thus, the hypomorphic *Icmt* allele partially mislocalizes prelamin A away from the nuclear rim but has no effect on the absolute levels of prelamin A.

Fibroblasts from *Zmpste24*$^{-/-}$ mice proliferate slowly and undergo premature senescence (19, 20). We defined the impact of *Icmt* deficiency on those phenotypes. As expected, *Zmpste24*$^{-/-}$*Icmt*$^{+/+}$ fibroblasts proliferated slowly and senesced prematurely (Fig. 3A). In contrast, *Zmpste24*$^{-/-}$*Icmt*$^{hm/hm}$ and *Zmpste24*$^{-/-}$*Icmt*$^{Δ/Δ}$ cells proliferated at rates similar to those of wild-type cells (Fig. 3A). Inactivating Fntb abolished cell proliferation (fig. S8).

We next explored the impact of *Icmt* deficiency on intracellular signaling pathways. The AKT-mTOR signaling pathway affects cell growth and survival (21). We observed higher levels of phosphorylated AKT and greater mTOR activation in *Zmpste24*$^{-/-}$*Icmt*$^{hm/hm}$ cell lysates than in *Zmpste24*$^{-/-}$*Icmt*$^{+/+}$ lysates, evident by increased phosphorylation of its downstream targets ribosomal protein S6 and 4E-BP1 (Fig. 3B). Similar results were observed in comparisons of *Zmpste24*$^{+/+}$*Icmt*$^{hm/hm}$ and *Zmpste24*$^{+/+}$*Icmt*$^{+/+}$ cells (fig. S9A). Consistent with increased rates of proliferation, *Zmpste24*$^{-/-}$*Icmt*$^{hm/hm}$ cells had lower levels of the cyclin-dependent kinase inhibitors p27^{KIP1} and p21^{CIP1} and the tumor suppressors p16^{INK4A} and phosphorylated retinoblastoma protein (Rb) (Fig. 3C). Levels of phospho-AKT and -S6 were lower in tissue lysates of *Zmpste24*$^{-/-}$*Icmt*$^{+/+}$ mice than in *Zmpste24*$^{+/+}$*Icmt*$^{+/+}$ mice; the levels were normalized in *Zmpste24*$^{-/-}$*Icmt*$^{hm/hm}$ tissues (fig. S9, B to D). Cytosolic phospho-AKT can translocate into the nucleus and trigger inactivation and degradation of p21^{CIP1} (21). Levels of phospho-AKT were high in nuclei of *Zmpste24*$^{-/-}$*Icmt*$^{hm/hm}$ hepatocytes and correlated with reduced levels of nuclear p21^{CIP1} (fig. S9E).

To determine whether increased AKT-mTOR signaling contributes to the increased proliferation of *Zmpste24*$^{-/-}$*Icmt*$^{hm/hm}$ cells, we performed cell proliferation assays with inhibitors of AKT (GSK690693) and mTOR (rapamycin). The AKT inhibitor blocked the proliferation of *Zmpste24*$^{-/-}$*Icmt*$^{hm/hm}$ cells, whereas the mTOR inhibitor had no effect (Fig. 3D and fig. S10, A to C). We also activated AKT in *Zmpste24*$^{-/-}$*Icmt*$^{+/+}$ cells with VO-OHpic, an inhibitor of phosphatase and tensin homolog (PTEN, a tumor suppressor upstream of AKT). VO-OHpic delayed the senescence of *Zmpste24*$^{-/-}$*Icmt*$^{+/+}$ cells (Fig. 3E and fig. S10D). Thus, *Icmt* deficiency overcomes senescence of *Zmpste24*$^{-/-}$ cells by activating AKT.

The increased AKT-mTOR signaling in *Icmt*-deficient cells was likely not caused by reduced methylation of RAS and RAS homologue enriched in the brain (RHEB) because their levels were unaffected by *Icmt* deficiency (fig. S11A). To test the possibility that the increased AKT-mTOR signaling was caused by unmethylated prelamin A, we analyzed fibroblasts from $Icmt^{hm/hm}$ mice on a background of a mutant *Lmna* allele ($Lmna^{LCO}$) that produces lamin C but no prelamin A (22). The levels of phospho-AKTand -S6 were lower in $Icmt^{hm/hm}Lmna^{LCO/LCO}$ lysates than in $Icmt^{hm/hm}Lmna^{+/+}$ lysates (fig. S11B). Thus, prelamin A is required for the increased AKT-mTOR signaling accompanying *Icmt* deficiency. Prelamin A and AKT were physically associated in $Zmpste24^{-/-}Icmt^{+/+}$ lysates; the association was reduced in $Zmpste24^{-/-}Icmt^{hm/hm}$ lysates (Fig. 3F). Perhaps an interaction between prelamin A and AKT in *Zmpste24*-deficient cells inhibits AKT-mTOR signaling (fig. S9, B to E).

To assess the effect of inhibiting *Icmt* in human fibroblasts, we suppressed ICMT expression in wild-type and HGPS fibroblasts with lentiviral short hairpin (sh) RNAs. The shRNAs reduced ICMT expression by 80% and had no discernible effect on the proliferation of fibroblasts from healthy subjects (Fig. 4A and fig. S12A). However, knockdown of ICMT in three HGPS cell lines delayed senescence and increased the mean proliferation rate (Fig. 4B and fig. S12B). The proliferation of HGPS cells also increased when ICMT activity was inhibited with *N*-acetyl-*S*-farnesyl-L-cysteine (AFC), a competitive ICMT inhibitor (fig. S12C). Rapamycin and an FTI dose-dependently reduced the proliferation of HGPS cells (fig. S12, D to G). The absolute levels of progerin were similar in shICMT-treated and control-HGPS cells, and phospho-AKT and -S6 levels were higher in shICMT-treated cells (Fig. 4C). Nuclear shape abnormalities in HGPS cells were unaffected by knockdown of ICMT (Fig. 4, D and E). Thus, cells from HGPS patients and *Zmpste24*-deficient mice respond similarly to ICMT inhibition.

Our findings raise the possibility that targeting *Icmt* could be an effective strategy for treating HGPS. Reduced ICMT expression was accompanied by improved disease phenotypes in $Zmpste24^{-/-}$ mice. Thus, the favorable effects in the setting of a hypomorphic *Icmt* allele suggest that the efficacy of ICMT inhibitors would not require complete inhibition of the enzyme.

Supplementary Material

Refer to Web version on PubMed Central for supplementary material.

Acknowledgments

We thank the Proteomics and Imaging Core Facilities at the Sahlgrenska Academy; M. Dalin, P. Lindahl, and J. Nilsson for comments; C. Karlsson and P. Iranmanesh for technical assistance; and S. Ordway for editing the manuscript. This study was supported by a Starting Investigator Grant from the European Research Council; and by grants from the Swedish Cancer Society, the Swedish Research Council, the Swedish Children's Cancer Fund, Västra Götalandsregionen, and the Ingabritt and Arne Lundberg's Research Foundation (to M.O.B). Data are available in the supplementary materials.

References and Notes

1. Davies BS, Fong LG, Yang SH, Coffinier C, Young SG. Annu. Rev. Genomics Hum. Genet. 2009; 10:153. [PubMed: 19453251]
2. Worman HJ, Fong LG, Muchir A, Young SG. J. Clin. Invest. 2009; 119:1825. [PubMed: 19587457]
3. De Sandre-Giovannoli A, et al. Science. 2003; 300:2055. [PubMed: 12702809]
4. Eriksson M, et al. Nature. 2003; 423:293. [PubMed: 12714972]
5. Yang SH, et al. Proc. Natl. Acad. Sci. U.S.A. 2005; 102:10291. [PubMed: 16014412]
6. Toth JI, et al. Proc. Natl. Acad. Sci. U.S.A. 2005; 102:12873. [PubMed: 16129834]
7. Young SG, Fong LG, Michaelis S. J. Lipid Res. 2005; 46:2531. [PubMed: 16207929]
8. Fong LG, et al. Science. 2006; 311:1621. [PubMed: 16484451]
9. Yang SH, et al. J. Clin. Invest. 2006; 116:2115. [PubMed: 16862216]
10. Yang SH, Qiao X, Fong LG, Young SG. Biochim. Biophys. Acta. 2008; 1781:36. [PubMed: 18082640]
11. Couzin-Frankel J. Science. 2012; 337:1594. [PubMed: 23019622]
12. Gordon LB, Cao K, Collins FS. J. Cell Biol. 2012; 199:9. [PubMed: 23027899]
13. Michaelson D, et al. Mol. Biol. Cell. 2005; 16:1606. [PubMed: 15659645]
14. Bergo MO, et al. J. Clin. Invest. 2004; 113:539. [PubMed: 14966563]
15. Svensson AW, Casey PJ, Young SG, Bergo MO. Methods Enzymol. 2006; 407:144. [PubMed: 16757321]
16. Bergo MO, et al. Proc. Natl. Acad. Sci. U.S.A. 2002; 99:13049. [PubMed: 12235369]
17. Fong LG, et al. Proc. Natl. Acad. Sci. U.S.A. 2004; 101:18111. [PubMed: 15608054]
18. Pendás AM, et al. Nat. Genet. 2002; 31:94. [PubMed: 11923874]
19. Varela I, et al. Nature. 2005; 437:564. [PubMed: 16079796]
20. Liu B, et al. Nat. Med. 2005; 11:780. [PubMed: 15980864]
21. Manning BD, Cantley LC. Cell. 2007; 129:1261. [PubMed: 17604717]
22. Fong LG, et al. J. Clin. Invest. 2006; 116:743. [PubMed: 16511604]

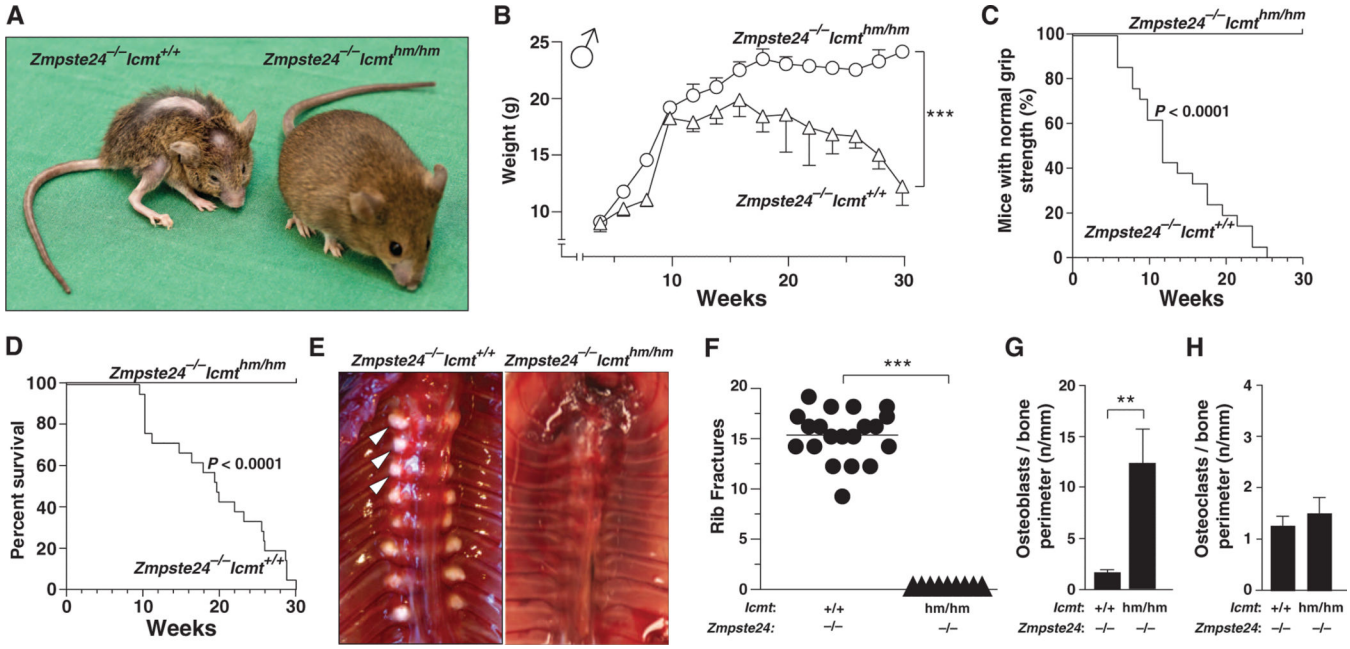

Fig. 1. Targeting Icmt ameliorates disease phenotypes and prevents death in 30-week-old *Zmpste24*$^{-/-}$ mice

(A) Photograph of 24-week-old littermate mice. **(B)** Body-weight curves of male *Zmpste24*$^{-/-}$*Icmt*$^{+/+}$ (n = 11) and *Zmpste24*$^{-/-}$*Icmt*$^{hm/hm}$ (n = 5) mice. **(C)** Kaplan-Meier plot showing the percentage of *Zmpste24*$^{-/-}$*Icmt*$^{+/+}$ (n = 21) and *Zmpste24*$^{-/-}$*Icmt*$^{hm/hm}$ (n = 9) mice with normal grip strength. **(D)** Kaplan-Meier plot showing survival of *Zmpste24*$^{-/-}$*Icmt*$^{+/+}$ (n = 21) and *Zmpste24*$^{-/-}$*Icmt*$^{hm/hm}$ (n = 9) mice. **(E)** Ventral view of spinal columns from an 18-week-old *Zmpste24*$^{-/-}$*Icmt*$^{+/+}$ mouse and a 30-week-old *Zmpste24*$^{-/-}$*Icmt*$^{hm/hm}$ mouse. Arrowheads indicate rib fractures at costovertebral joints. **(F)** Number of rib fractures in *Zmpste24*$^{-/-}$*Icmt*$^{+/+}$ (n = 21) and *Zmpste24*$^{-/-}$*Icmt*$^{hm/hm}$ (n = 9) mice. (**G** and **H**) Cellular parameters of L2 vertebrae (n = 6 per genotype). $^{**}P < 0.01$; $^{***}P < 0.001$. Data are presented as mean ± SEM.

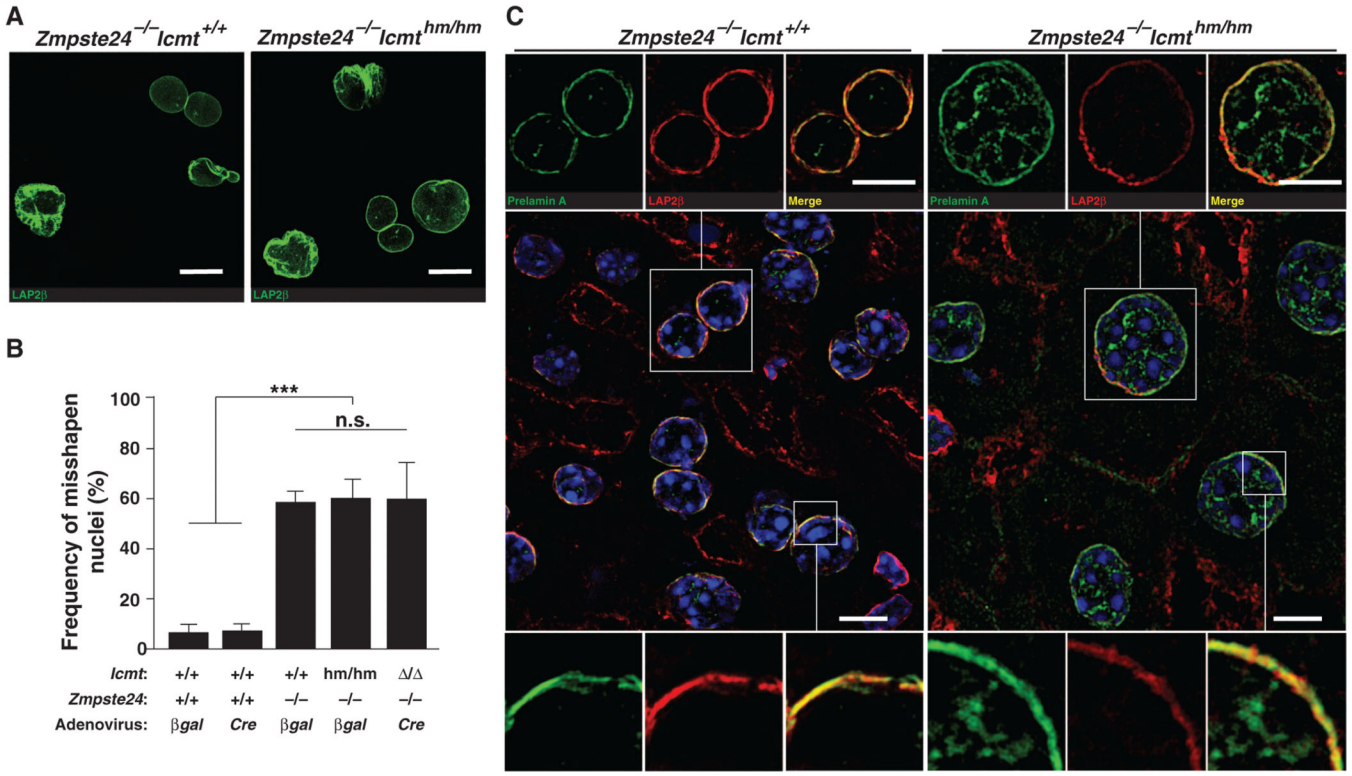

Fig. 2. *Icmt* deficiency mislocalizes prelamin A but does not reduce the frequency of misshapen nuclei in *Zmpste24*$^{-/-}$ fibroblasts

(A) Confocal images of nuclei in primary mouse embryonic fibroblasts stained with a LAP2b antibody. Scale bar, 10 μm. **(B)** Frequency of misshapen nuclei in primary fibroblasts (n = 3 per genotype). Cre-adenovirus was used to produce *Zmpste24*$^{-/-}$*Icmt*$^{\Delta/\Delta}$ cells from the parental *Zmpste24*$^{-/-}$*Icmt*$^{hm/hm}$ cells. β*gal*-adenovirus was used as control. **(C)** Super-resolution structured illumination microscopy (SR-SIM) immunofluorescence images of nuclei in liver sections stained with prelamin A– and LAP2β-specific antibodies and counterstained with 4', 6-diamidino-2-phenylindole (DAPI). Scale bar, 10 μm. ***P < 0.001.

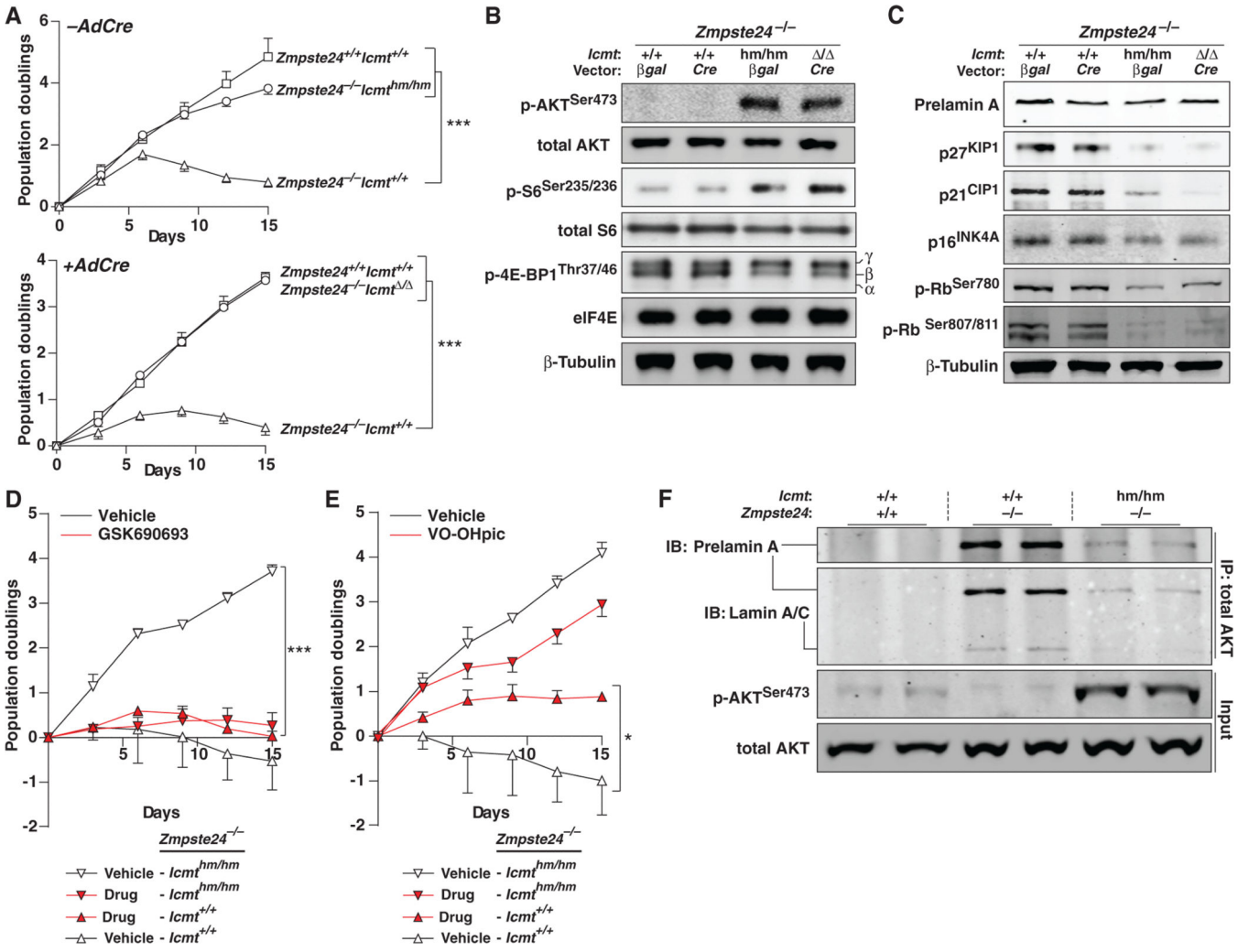

Fig. 3. *Icmt* deficiency prevents premature senescence of *Zmpste24*$^{-/-}$ fibroblasts by increasing AKT pathway signaling

(A) Growth curves of primary fibroblasts (n = 4 per genotype) before (top) and after (bottom) incubation with *Cre*-adenovirus. *(B)* Immunoblots of fibroblast extracts show increased phosphorylation of AKT, S6, and 4E-BP1. Increased phosphorylation and inactivation of 4E-BP1 is evident by an increased ratio of γ and β/α isoforms. eIF4E and β-tubulin were the loading controls. **(C)** Immunoblots of fibroblast extracts with antibodies against prelamin A and cell cycle regulatory proteins. (**D** and **E**) Growth curves of primary fibroblasts incubated with inhibitors of (D) AKT (GSK690693, 10 μM) and (E) PTEN (VO-OHpic, 150 nM) (n = 3/genotype). **(F)** Immunoprecipitation (IP) and immunoblot (IB) analyses showing a methylation-dependent association between AKT and prelamin A. The lysates were also used directly for immunoblots for AKT (input). *P < 0.05; ***P < 0.001.

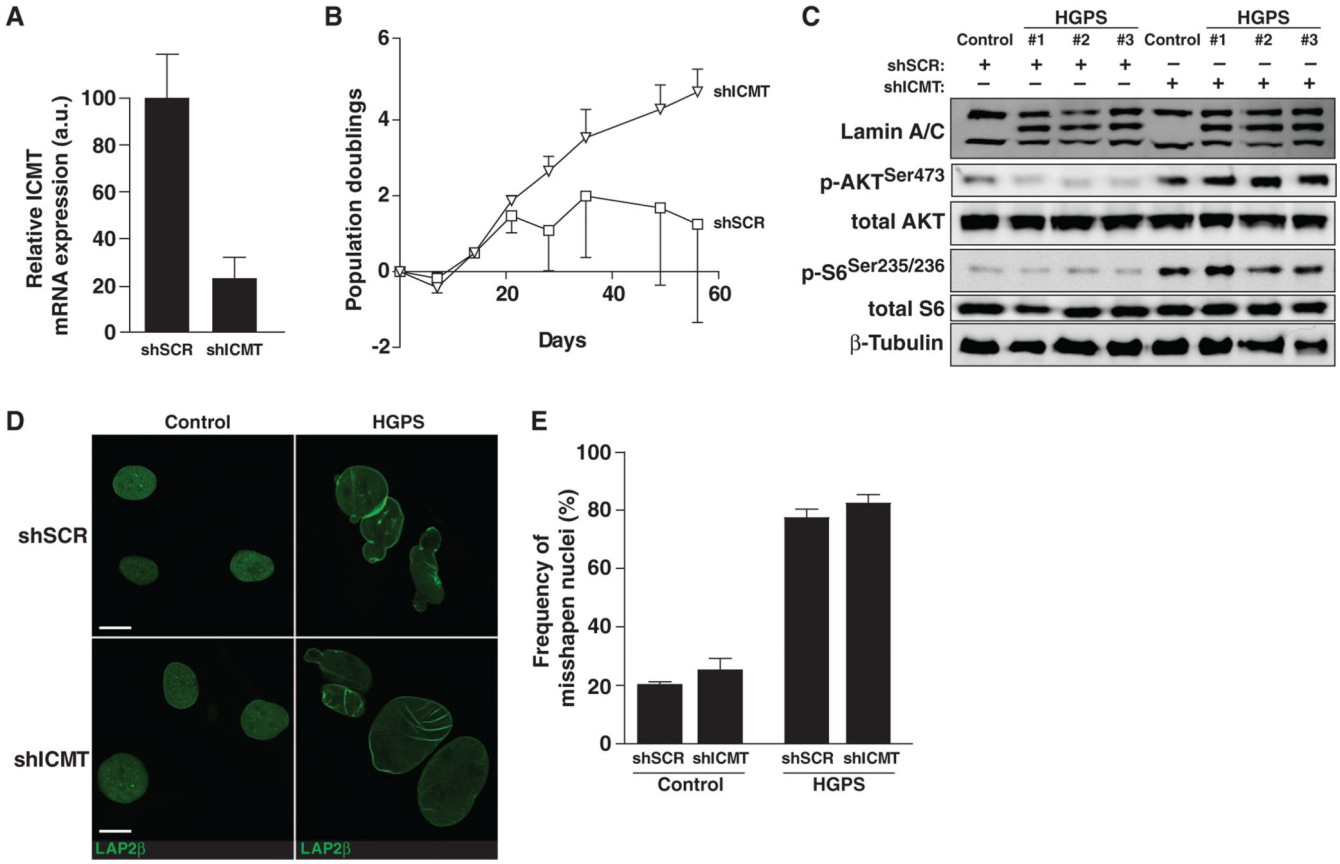

Fig. 4. *Icmt* knockdown in human HGPS fibro-blasts prevents premature senescence and increases AKT-mTOR pathway signaling

(A) TaqMan analyses showing *ICMT* mRNA levels in skin fibro-blasts from HGPS patients incubated with shRNA lentiviruses. Data are means of three independent cell lines incubated with two lentiviral clones expressing ICMT shRNAs or with a control clone containing a scrambled (SCR) sequence. **(B)** Growth curves of HGPS cells incubated with shIcmt or shSCR lentiviruses (n = 3 cell lines per treatment). **(C)** Immunoblots of fibroblast extracts; β-tubulin was the loading control. **(D)** Confocal images of fibroblasts stained with an antibody against LAP2b. Scale bar, 10 μm. **(E)** Frequency of nuclear shape abnormalities in control and HGPS fibroblasts incubated with shICMT and shSCR lentiviruses (n = 3 cell lines per treatment).